

SEMPA STUDIES OF OSCILLATORY EXCHANGE COUPLING

John Unguris, Daniel T. Pierce, Robert J. Celotta, and
Joseph A. Stroscio

National Institute of Standards and Technology
Gaithersburg, MD 20899

ABSTRACT

We have used scanning electron microscopy with polarization analysis (SEMPA) to investigate the magnetic exchange coupling between an Fe film and an Fe whisker separated by either a Cr or Ag spacer layer. The thickness dependence of the oscillatory coupling in these atomically well ordered, epitaxial films was precisely measured. The periodicity of the exchange coupling is consistent with predictions based on Fermi surface spanning vectors of the interlayer material.

INTRODUCTION

The exchange coupling between magnetic layers separated by nonmagnetic layers oscillates between ferromagnetic (FM) and antiferromagnetic (AFM) coupling as a function of the spacer layer thickness in a wide variety of systems.¹ The strength and periodicity of this oscillatory exchange coupling depends sensitively upon the atomic order in the films. While most polycrystalline exchange coupled films seem to show an oscillation period of about 1 nm,² well-ordered, single crystal films exhibit more complex, sometimes multi-periodic behaviors.³⁻¹⁰ The origin of the coupling and the factors that determine the period of the oscillations in the coupling are subjects of intense interest, as is the technologically important spin-valve magnetoresistance observed in multilayers of these materials. The goal of this work is to provide precise measurements of the oscillation periods in high quality films in order to better couple theory with experiment.

In this article, we describe measurements for two different sandwich structures where the spacer materials are either a transition metal, Cr, or a noble metal, Ag. The spacer films are deposited on nearly perfect, single crystal Fe whisker substrates and covered with a thin Fe film. The atomic structure of the films is characterized by reflection high energy electron diffraction (RHEED) and scanning tunneling microscopy (STM). The magnetization of the films is measured with scanning electron microscopy with polarization analysis (SEMPA). For both spacer layers, the oscillatory exchange coupling consists of both short and long period contributions, and the oscillations persist over at least 10 nm of spacer material. In each case the observed periodicities are consistent with models of

the exchange coupling in which spanning vectors of the spacer layer's Fermi surface dominate the magnetic response of the multilayer.

EXPERIMENT

The experimental procedures used to investigate the Fe/Cr/Fe and Fe/Ag/Fe structure have been previously described.^{3,4} The magnetization, crystalline order, and chemical composition are measured using SEMPA,¹¹ RHEED, and scanning Auger microscopy, respectively. All of this analysis is done *in situ* and, when necessary, during film evaporation. In addition, STM measurements of the atomic scale order were made using similar Fe whisker substrates in a separate experiment. The use of high spatial resolution analytical techniques allows us to study films that are grown on Fe whisker substrates that are only a few tenths of a mm across by one cm long. The Fe whiskers are extremely high quality, strain free crystals with very low dislocation densities.¹² The whisker surfaces are naturally flat and can be prepared by well established ion sputtering and heating procedures.¹³ STM measurements of Fe(100) whisker surfaces show atomically flat terraces that are separated by single atom high steps that are at least $1 \mu\text{m}$ apart.¹⁴ RHEED patterns from the whiskers show sharp diffraction spots distributed along Laue rings.

In order to measure the exchange coupling as a continuous function of spacer layer thickness, a wedge shaped interlayer was grown on the Fe substrate. A schematic of the wedge is shown in Fig. 1. We obtained the wedge shape by moving a precision, piezo-controlled shutter during the evaporation. The slope of the wedge is very small, between 0.001° and 0.0001° . The thickness of the spacer layer is determined by measuring RHEED intensity oscillations as the focused electron beam is scanned along the wedge. Using spatially resolved RHEED to measure the thickness eliminates any errors due to drifting evaporation rates or local thickness variations arising from microscopic defects in the shutter.

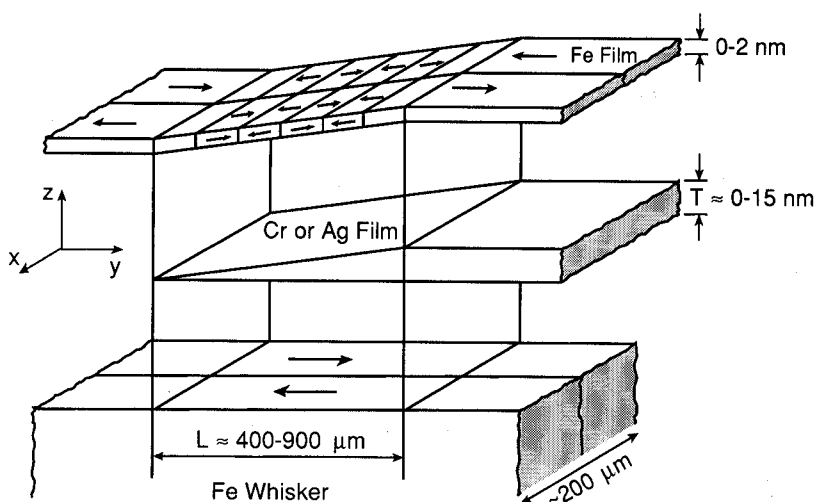


Fig. 1. A schematic exploded view of the sample structure showing the Fe(001) single-crystal whisker substrate, the evaporated Cr wedge, and the Fe overlayer. The arrows in the Fe show the magnetization direction in each domain. The z-scale is expanded approximately 5000 times.

The magnetic coupling between the Fe(100) substrate and Fe film overcoat are determined using SEMPA.³ Specifically, SEMPA measures the spin polarization of the secondary electrons which, for a simple transition metal ferromagnet, is directly proportional to the magnetization. A coupling measurement therefore simply involves measuring the direction of the magnetization in the Fe overcoat and comparing it to the magnetization of the bare Fe substrate. In these measurements we assume that the magnetization of the Fe whisker is unchanged. The escape depth of the secondary electrons is about 1 nm so that only the magnetization of the outermost layers is measured. Possible instrumental offsets in the SEMPA measurements are determined and eliminated by only using Fe whiskers that are divided lengthwise into two oppositely magnetized domains. Finally, it should be noted that SEMPA does not directly measure the magnitude of the exchange coupling, but it is extremely sensitive to the direction of the magnetic coupling in these multilayer systems.

Cr RESULTS

Both Cr and Fe are body centered cubic crystals with only a 0.7% lattice mismatch, and the surface free energy of Cr is less than that of Fe. Therefore one should expect Cr to grow in a layer by layer mode on Fe. Experimentally, we find that the growth is strongly temperature dependent so that temperatures in the range of 250°C to 350°C are required in order to achieve true layer by layer growth. The temperature dependence of the growth is illustrated in Fig. 2 in which STM images of bare Fe(100) and of Cr films grown at various temperatures are shown. The STM image of the Cr film grown at 100°C, Fig. 2(b) shows that the growth front extends over at least four layers. The corresponding RHEED pattern from the 100°C Cr film shows weak diffraction spots, enhanced diffuse scattering and transmission diffraction features characteristic of a rough sample. In contrast, the RHEED pattern from the Cr film grown at 300°C is almost as sharp as the bare Fe RHEED pattern and the STM image, Fig. 2(c), shows a nearly ideal growth front with only two layers participating.

The temperature dependence of the Cr growth has a dramatic effect on the Fe/Cr/Fe magnetic exchange coupling.³ Fig. 3 shows SEMPA images of the magnetic domain structure in the bare Fe whisker and in an Fe film deposited on top of Cr wedges that were grown at 30°C, Fig. 3(b), and 350°C, Fig. 3(c). These SEMPA images show the magnetization component along the whisker; white corresponds to magnetization pointing towards the right and black to the left. The oscillatory exchange coupling is clearly present for both Cr wedges and in both cases the oscillations persist for at least 10 nm, but the periodicity of the coupling is very different. While the coupling through Cr grown at the lower temperature oscillates with a period of 11-13 layers (1.6-1.9 nm), the coupling through Cr grown at higher temperature changes, after the initial 5 layer FM coupling region, with each layer of Cr giving an oscillation period of nearly two layers. We say "nearly" because at 24-25, 44-45, and 64-65 layers, indicated by the arrows at the top of the figure, no reversal takes place. This corresponds to a phase slip resulting from the accumulation of a phase difference owing to the incommensurability of the exchange period and the lattice constant. The actual period of the short period oscillations at room temperature is therefore 2.11 ± 0.03 Cr layers (0.304 ± 0.004 nm).

Further evidence for the correlation between short period oscillations and Cr film quality can be obtained by comparing the coupling measurements with RHEED intensity oscillations measurements. An example of the correlation between RHEED intensity oscillations and short period oscillations is shown in Fig. 4. The RHEED image is obtained by measuring the intensity of the specular RHEED beam as the incident electron

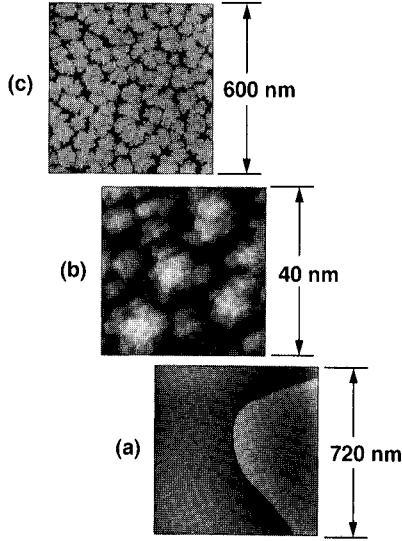


Fig. 2 STM images of (a) a clean Fe whisker substrate with a single, one Cr atom high step, (b) a Cr film deposited on an Fe whisker at 100°C showing the rough, multilevel surface, and (c) a Cr film deposited at 300°C showing a nearly ideal 2 layer growth front. The size of the scanned area is given to the right of each image.

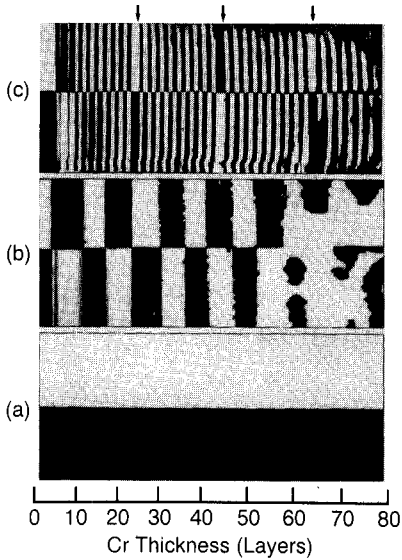


Fig. 3. SEMPA image of the magnetization M_y (axes as in Fig. 7) showing domains in (a) the clean Fe whisker, (b) the Fe layer covering the Cr spacer layer evaporated at 30°C, and (c) the Fe layer covering a Cr spacer evaporated on the Fe whisker held at 350°C. The scale at the bottom shows the increase in the thickness of the Cr wedge in (b) and (c). The region of the whisker imaged is about 0.5 mm long. The Cr thicknesses at which exchange coupling phase slips occur are indicated by the arrows at the top of the figure.

beam is rastered over an uncovered Cr wedge that was grown at 250°C. We attribute the absence of RHEED oscillations in the thicker part of the wedge to roughness of the Cr film, possibly caused by the slightly less than optimal growth temperature and damage in the Fe substrate from too many sputtering and annealing cycles. The important point to note, however, is that in the magnetization image of the Fe overlayer, M_y , the coupling reverts to long period oscillatory coupling at the same thickness that the RHEED intensity oscillations disappear.

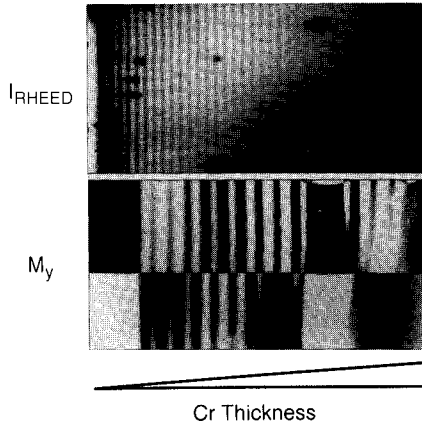


Fig. 4. The effect of roughness on the interlayer exchange coupling is shown by a comparison of the oscillations of the RHEED intensity along the bare Cr wedge with the SEMPA M_y magnetization image over the same part of the wedge.

It is noteworthy that a calculation of the exchange coupling in Fe/Cr/Fe predicted short period oscillations, in addition to the long period oscillations, before short period oscillations had been observed experimentally. Wang et al¹⁵ pointed out that the apparent discrepancy with earlier experiments, which showed no short period oscillations, could be accounted for by interfacial roughness corresponding to the displacement of one quarter of the atoms in the interface by one layer. For a Cr film n layers thick, this roughness corresponds to 25% of the surface being at $n-1$ layers, 50% at n layers, and 25% at $n+1$ layers. This is equivalent to a three layer growth front with 0.10 nm rms roughness. Therefore, in order to observe the short period oscillations, the Cr must grow in nearly an ideal layer by layer manner where one layer is completed before the next layer begins.

Data from the SEMPA and scanned RHEED images can be used to take a more quantitative look at the Cr thickness dependence of the exchange coupling. Fig. 5 shows the polarization of the bare Cr, $P(\text{Cr})$, compared with the polarization of the same wedge after coating it with a thin (~ 1 nm thick) Fe film. The Cr thickness scale is calibrated using the RHEED intensity oscillations shown at the top of Fig 5. The RHEED measurements were made near the out of phase diffraction condition where peaks in the specular intensity correspond to filled layers. The RHEED and SEMPA measurements are

registered by aligning defects, usually found near the edge of the whisker, that appear in both the RHEED and SEMPA intensity images. The build-up of disorder and roughness with increasing Cr thickness is indicated by the corresponding decrease in the amplitude of the RHEED intensity oscillations.

The measured spin polarization of secondary electrons from the bare Cr, before and after removing the background polarization from the Fe substrate, is shown in the middle of Fig. 5. The high polarization of electrons from the Fe at the start of the wedge decreases exponentially as the Fe electrons are attenuated by the Cr film of increasing thickness. A fit to the exponential gives a $1/e$ sampling depth for SEMPA in Cr of 0.55 ± 0.05 nm. Subtracting the exponential background leaves the Cr polarization, $P(\text{Cr})$, which is shown magnified by a factor of 5. Because of the attenuation of the electrons coming from layers below the surface, $P(\text{Cr})$ is dominated by the polarization of the surface layer which is seen to reverse nearly every layer.

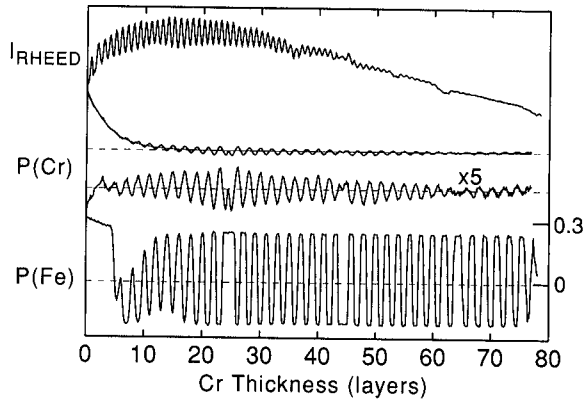


Fig. 5. Scanned RHEED and SEMPA measurements from the same Cr wedge showing the thickness dependence of the RHEED intensity oscillations (top), the spin polarization of secondary electrons emitted from the bare Cr, $P(\text{Cr})$, before and after removing the Fe substrate polarization (middle), and the M_y polarization component from an Fe layer, $P(\text{Fe})$, deposited on top of the Cr (bottom).

After coating this Cr wedge with a 5 layer thick Fe film a SEMPA measurement yields the thickness dependence of the magnetic coupling shown in the bottom of Fig. 5. The polarization of the Fe overlayer, $P(\text{Fe})$, is seen to be opposite to that of the top layer of the bare Cr. This observation is consistent with spin-polarized photoemission¹⁶ and electron energy loss¹⁷ measurements which have shown that the Fe-Cr interface is antiferromagnetically coupled. In addition, the phase slips at 24-25, 44-45, and 64-65 layers are seen in both $P(\text{Cr})$ and $P(\text{Fe})$. With AFM coupling at each interface and if the Cr orders antiferromagnetically with successive planes of reversed moments in the [100] direction, one expects the Fe/Cr/Fe coupling for even numbered layers of Cr to be AFM, and FM for odd numbers of Cr layers. However, looking at $P(\text{Fe})$ we see that Fe separated by 7 layers of Cr is antiferromagnetically coupled, opposite to expectations. A close examination of $P(\text{Cr})$ reveals that there is a defect in the AFM layer stacking of Cr between 1 and 4 layers. That is, at a thickness of less than four layers, adjacent layers of Cr must have parallel moments.

One might argue that the observation of short period oscillatory coupling through Cr interlayers is not surprising, since bulk Cr is a spin density wave (SDW) antiferromagnet

so that the coupling is simply an extension of the antiferromagnetic stacking. However, the SDW and the oscillatory exchange coupling have the same origin. The SDW arises from an enhanced susceptibility at a wave vector that spans extended parallel regions of the Cr Fermi surface. Cr is special in that there is a strong "nesting" of the Fermi surface.¹⁸ This same enhanced susceptibility at a particular spanning wave vector is also responsible for the short period oscillations in Ruderman-Kittel-Kasuya-Yosida (RKKY)-like models of the Fe/Cr/Fe exchange coupling through paramagnetic Cr interlayers. This makes it hard to distinguish between an RKKY-like coupling and an explanation where the Fe magnetization is locked to the antiferromagnetism of the Cr. In an attempt to differentiate between these two mechanisms we have measured the temperature dependence of $P(\text{Cr})$ and $P(\text{Fe})$.¹⁹ We find that the oscillatory coupling, along with the phase slips associated with the SDW, persist from just below the Néel temperature, $T_N=38^\circ\text{C}$, to $1.8 T_N$. Above T_N bulk Cr is paramagnetic which suggests that either the coupling takes place through paramagnetic Cr or that the presence of the Fe substrate stabilizes the antiferromagnetism in Cr. We therefore have two closely related ways to view this response in the Cr film. In one view, since even above T_N the magnetic susceptibility is enhanced at the nesting wavevector, an antiferromagnetic response can be induced in the Cr by the presence of the Fe. Alternatively, if the Cr is viewed as a paramagnet, RKKY-like oscillations would be established which would be quite similar to the antiferromagnetic order because both derive from the same strong Fermi surface nesting.

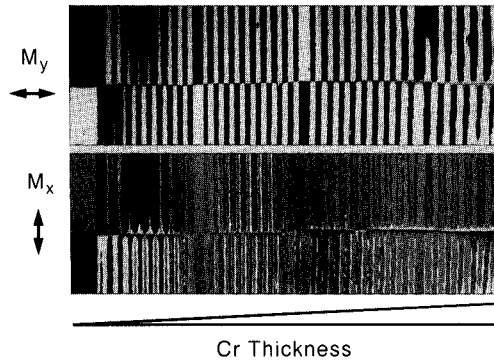


Fig. 6. SEMPA images from a Fe/Cr/Fe(100) wedge showing the M_y and M_x magnetization components. The presence of biquadratic coupling can be seen by the increased contrast of M_x at the FM/AFM transitions.

Finally, one should note that the exchange coupling in Fe/Cr/Fe is not purely FM or AFM, but there can also be an in-plane component that is not parallel or antiparallel to the substrate magnetization. Phenomenologically this additional coupling may be treated as a higher order term in an expansion of the exchange coupling energy per unit area,²⁰

$$E = A_{12}[1 - \mathbf{m}_1 \cdot \mathbf{m}_2] + \frac{1}{2}B_{12}[1 - (\mathbf{m}_1 \cdot \mathbf{m}_2)^2]$$

where \mathbf{m}_1 and \mathbf{m}_2 are unit vectors in the direction of magnetization in the two Fe layers,

A_{12} is the coefficient of the bilinear coupling term which yields either FM or AFM alignment, and B_{12} is coefficient of biquadratic coupling which favors an orthogonal magnetization. Biquadratic coupling in Fe/Cr/Fe was initially observed in a magneto-optic Kerr microscopy investigation.²⁰ In the SEMPA measurements, the biquadratic coupling can be most clearly seen in images of the in-plane magnetization component that is orthogonal to the FM/AFM axis. Fig. 6 shows images of both in-plane magnetization components for an Fe/Cr/Fe(100) wedge. M_y is the magnetization component along the whisker magnetization axis, while M_x is the simultaneously measured orthogonal component. The large contrast in M_x at the FM/AFM transitions shows that the biquadratic coupling dominates the bilinear at these thicknesses. The width of these transition zones is proportional to the strength of the biquadratic coupling relative to the bilinear.²⁰ Note that the transition zones are not simply domain walls in the Fe film, since they are much wider than the domain walls in Fe and they scale inversely with the slope of the wedge. The physical origin of the biquadratic exchange coupling is still not well understood. Both intrinsic²¹ and extrinsic²² origins for the coupling have been proposed.

Ag RESULTS

Unlike Cr with its complex Fermi surface and its SDW antiferromagnetism, Ag is diamagnetic and has a relatively simple Fermi surface. In this regard Ag is a better interlayer material for testing models of the oscillatory exchange coupling. Unfortunately Ag is not as close a perfect epitaxial match to Fe as Cr is. The larger Ag fcc unit cell, when rotated by 45° in order to match the bcc Fe substrate, results in a lateral mismatch of only 0.8%, but, perpendicular to the surface, a single atom high Ag step is 42% larger than an Fe step. Ag only grows well over a narrow range of substrate temperatures and Ag evaporation rates, and Ag does not grow as well as Cr on Fe. Nevertheless our investigations of the exchange coupling in Fe/Ag/Fe(100) show oscillatory coupling for spacer films that are up to at least 50 Ag layers ($> 10\text{nm}$) thick.⁴

Fig. 7 shows a scanned RHEED image obtained from a bare Ag wedge and SEMPA images from the same sample after coating it with Fe. As in the Cr measurements, the thickness of the Ag wedge is measured using the intensity oscillations in the bare Ag RHEED image. M_y and M_x are the magnetization components along and orthogonal to the Fe whisker axis, respectively. The SEMPA images show that both long and short period oscillations contribute to the exchange coupling, although the short period contribution is much less pronounced when compared with that of the Cr interlayers. The M_x image shows that there is also a significant biquadratic coupling contribution to the exchange coupling. The relative strength of the biquadratic coupling appears to increase with increasing Ag thickness, since the widths of the FM/AFM transitions increase in the thicker part of the Ag wedge. Fig. 8 shows averaged line scans of M_y and M_x and the derived angle of the in-plane magnetization, Θ , obtained from the images in Fig. 7 and plotted as a function of the Ag thickness.

In order to extract the coupling periods from the Fe/Ag/Fe(100) SEMPA data, we model the magnetization by adding together two sine waves with adjustable periods, phases, and amplitudes. This coupling function is discretized at the Ag lattice and then all positive coupling values are set to the same magnetization and all negative values are set to the equal but opposite magnetization. The coupling periods determined by varying the parameters to achieve the best fit are 5.73 ± 0.05 Ag layers (1.17 ± 0.01 nm) and 2.37 ± 0.07 Ag layers (0.485 ± 0.014 nm).

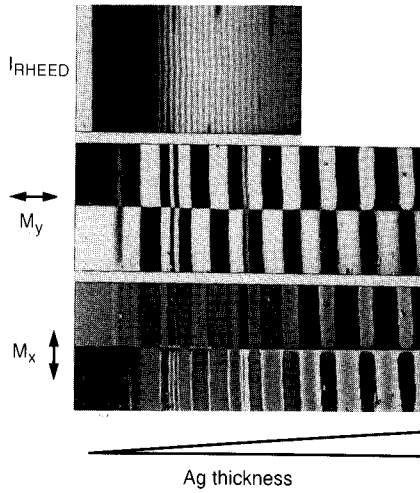


Fig. 7. A scanned RHEED image of a bare Ag wedge, and SEMPA images, showing the in-plane magnetization components, M_y and M_x , of the same wedge after coating it with three layers of Fe. The RHEED image was used to calibrate the Ag thickness.

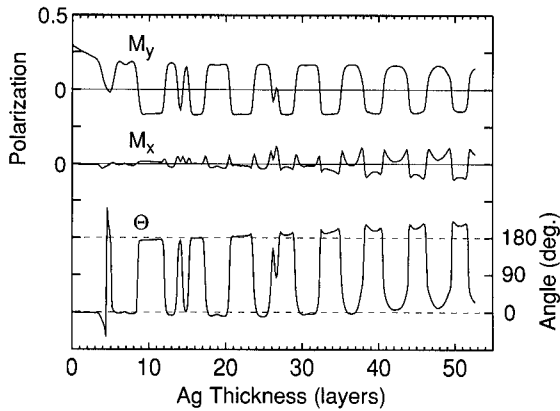


Fig. 8. The Ag thickness dependence of M_y , M_x and the in-plane magnetization angle, Θ , derived from the images in Fig. 7. The angle is plotted so that 0° (180°) corresponds to FM (AFM) coupling.

DISCUSSION AND CONCLUSION

Measurements of the oscillatory exchange coupling provide a test of various exchange coupling theories. In particular, for theories that are based on RKKY-type interactions, the coupling periodicities are closely related to the size and shape of the Fermi surface of the interlayer material. The periodicity of the oscillatory coupling is dominated by reciprocal lattice vectors that are perpendicular to the interface and span nearly parallel sections of the Fermi surface. The enhanced susceptibility of the spacer layer at these interface Fermi surface spanning vectors results in the oscillatory exchange coupling. A simple test of various coupling models, therefore, is to see how well they predict the observed periods of the oscillatory exchange coupling.

Table 1

Exchange Coupling Period (layers)					
		Fe/Cr/Fe(100) (0.144nm/layer)		Fe/Ag/Fe(100) (0.204nm/layer)	
Experiment		2.11±0.03	12±1	2.37±0.07	5.73±0.05
Theory	Bruno, Chappert ²³ Stiles ²⁴	2.10	11.3	2.38	5.58

Table I summarizes the Cr and Ag interlayer coupling periods and compares them with the results of two different derivations of Fermi surface spanning vectors. Bruno and Chappert²³ use De Haas-van Alphen and cyclotron resonance measurements of Fermi surface extremals as the basis for their Fermi surface calculations of the noble metals. Stiles²⁴ uses a tight-binding approximation to fit the band structure in order to calculate the Ag and Cr spanning vectors. In the case of Cr, it is clear that the short period oscillations are related to the spanning vector that bridges the unusually strong nesting feature of the Cr Fermi surface. This is the same Fermi surface nesting feature that leads to the enhanced susceptibility and the related SDW antiferromagnetism in Cr. The origin of the long period oscillation in Cr is less clear, however, since the complicated Cr Fermi surface has 10 other spanning vectors which also correspond to significant Fermi surface nesting. While one of these spanning vectors results in a period that is close to what we observe, it is not clear why we do not observe oscillatory coupling associated with the others. Roughness may play a role, as we have shown in the case of low temperature Cr growth. In addition, Fermi surface nesting only reveals which periodicities are possible, while the matrix elements, which have not as yet been calculated, determine the relative amplitudes of the various periodic contributions to the exchange coupling.

For Ag the comparison is easier since the Ag Fermi surface is less complex and only two spanning vectors are found which can lead to coupling in the [001] direction. Table I shows that the measured coupling periods are in excellent agreement with the theoretical values, considering possible uncertainties in the theory and the possibility of some slight tetragonal distortion of the strained Ag interlayer. The SEMPA measurements show that the oscillations of the interlayer coupling in Fe/Ag/Fe(100) are consistent with theories in which oscillation periods are derived from Fermi surface spanning vectors.

A common feature of both the Fe/Cr/Fe and Fe/Ag/Fe multilayer coupling investigations is the sensitivity of the exchange coupling to the quality of film growth. This work emphasizes that, in order to make meaningful and quantitative comparisons with theoretical predictions, coupling measurements must be made on interlayer films that are atomically well ordered and characterized. In this regard, SEMPA is especially well suited for measuring the coupling periodicities, because the high resolution of SEMPA permits the use of small, nearly perfect, single crystal Fe whisker substrates. SEMPA also has the surface sensitivity to interrogate only the top layer of the trilayer structures and it can be used in situ, along with RHEED and Auger spectroscopy, to study the multilayer structures as they are made. SEMPA measurements using Fe whisker substrates have given the most precise determination of the periods of oscillatory exchange coupling in Fe/Cr/Fe(100) and Fe/Ag/Fe(100), the two systems that have been studied by SEMPA to date, and the experimental results on Cr and Ag interlayers support theories of interlayer exchange coupling based on Fermi surface properties.

ACKNOWLEDGEMENTS

We wish to thank M. H. Kelley and M. D. Stiles for many helpful discussions. The Fe whiskers were grown at Simon Fraser University under an operating grant from the National Science and Engineering Research Council of Canada. This work is supported by the Office of Technology Administration of the Department of Commerce and by the Office of Naval Research.

REFERENCES

1. See review articles in "Ultrathin Magnetic Structures", (B. Heinrich and A. Bland, eds.), Springer Verlag, 1992.
2. S.S.P. Parkin, *Phys. Rev. Lett.* **67**, 3598 (1991).
3. J. Unguris, R.J. Celotta, and D.T. Pierce, *Phys. Rev. Lett.* **67**, 140 (1991).
4. J. Unguris, R.J. Celotta, and D.T. Pierce, to be published.
5. S. Demokritov, J.A. Wolf, P. Grünberg, and W. Zinn, in *Proc. Mats. Res. Soc. Symp.* **231**, 133 (1992).
6. S.T. Purcell, W. Folkerts, M.T. Johnson, N.W.E. McGee, K. Jager, J. aan de Stegge, W.B. Zeper, W. Hoving, and P. Grünberg, *Phys. Rev. Lett.* **67**, 903 (1991).
7. M.T. Johnson, S.T. Purcell, N.W.E. McGee, R. Coehoorn, J. aan de Stegge, and W. Hoving, *Phys. Rev. Lett.* **68**, 2688 (1992).
8. A. Fuss, S. Demokritov, P. Grünberg, and W. Zinn, *J. Mag. and Mag. Mat.* **103**, L221 (1992).
9. Z.Q. Qiu, J. Pearson, A. Berger, and S.D. Bader, *Phys. Rev. Lett.* **68**, 1398 (1992).
10. S.T. Purcell, M. T. Johnson, N.W.E. McGee, R. Coehoorn, and W. Hoving, *Phys. Rev.* **B45**, 13064 (1992).
11. M.R. Scheinfein, J. Unguris, M.H. Kelley, D.T. Pierce, and R.J. Celotta, *Rev. Sci. Instrum.* **61**, 2501 (1990).
12. P.D. Gorsuch, *J. Appl. Phys.* **30**, 837 (1959).
13. S.T. Purcell, A.S. Arrott, and B. Heinrich, *J. Vac. Sci. Technol.* **B6**, 794 (1988).
14. J. Stroschio, D.T. Pierce, J. Unguris, R.J. Celotta, and R.A. Dragoset, to be published.

15. Y. Wang, P.M. Levy, and J.L. Fry, Phys. Rev. Lett. **65**, 2732 (1990).
16. F.U. Hillebrecht, C. Roth, R. Jungblut, E. Kisker and A. Bringer, Europhys. Lett. **19**, 711 (1992).
17. T.G.Walker, A.W.Pang, H.Hopster, and S.F.Alvarado, Phys. Rev. Lett. **69**, 1121 (1992).
18. E. Fawcett, Rev. Mod. Phys. **60**, 209 (1988).
19. J. Unguris, R.J. Celotta, and D.T. Pierce, Phys. Rev. Lett. **69**, 1125(1992).
20. M. Rühlig, R. Schäfer, A. Hubert, R. Mosler, J.A. Wolf, S. Demokritov and P. Grünberg, phys. stat. sol. (a) **125**, 635 (1991).
21. R.P. Erickson, K.B. Hathaway, and J.R. Cullen, to be published.
22. J.C. Slonczewski, Phys. Rev. Lett. **67**, 3172 (1991).
23. P. Bruno and C. Chappert, Phys. Rev. Lett. **67**, 1602 (1991); Phys. Rev. **B46**, 261 (1992).
24. M.D. Stiles, to be published.